

Dynamical models and Galaxy surveys

James Binney¹ & Jason L. Sanders¹

¹ Rudolf Peierls Centre for Theoretical Physics, Keble Road, Oxford, OX1 3NP, UK
email: binney@thphys.ox.ac.uk, jason.sanders@physics.ox.ac.uk

Abstract. Equilibrium dynamical models are essential tools for extracting science from surveys of our Galaxy. We show how models can be tested with data from a survey before the survey's selection function has been determined. We illustrate the application of this method by presenting some results for the RAVE survey. We extend our published analytic distribution functions to include chemistry and fit the chosen functional form to a combination of the Geneva–Copenhagen survey (GCS) and a sample of G-dwarfs observed at $z \sim 1.75$ kpc by the SEGUE survey. By including solid dynamics we are able to predict the contribution that the thick disc/halo stars surveyed by SEGUE should make to the GCS survey. We show that the measured [Fe/H] distribution from the GCS includes many fewer stars at [Fe/H] < -0.6 than are predicted. The problem is more likely to lie in discordant abundance scales than with incorrect dynamics.

Keywords. stellar dynamics, surveys, stars: abundances, Galaxy: disk, Galaxy: kinematics and dynamics, Galaxy: stellar content

1. Introduction

Very significant resources are being invested in large surveys of the stellar content of our Galaxy. We clearly are under an obligation to make every effort to extract as much science from these expensive data as we can. A survey catalogue is always dominated by selection effects: it contains stars that are nearby and luminous. Moreover several of the quantities measured for stars, for example parallax ϖ , proper motion μ , α enhancement [α/Fe], contain non-negligible errors, and the quantities of physical interest that we derive from them, such as distance s , luminosity L and velocity \mathbf{v} , have correlated errors with highly non-Gaussian error distributions. Models play a vital role in extracting science from surveys by taking into account (i) selection effects (ii) measurement errors and (iii) combining constraints on the properties of the Galaxy from different surveys. Here we illustrate these principles.

2. Importance of equilibrium models

There is a long tradition of extracting science from surveys with kinematic models such as the Besançon model (Robin et al. 2003). These models are constructed by assigning to each spatial point a velocity ellipsoid, generally assumed to be Gaussian. Equilibrium dynamical models are superior to kinematic models in several ways.

- Although the Galaxy cannot be in dynamical equilibrium, equilibrium models are of fundamental importance because an estimate of the Galaxy's gravitational potential $\Phi(\mathbf{x})$ is key for any modelling enterprise and we can constrain Φ only to the extent that the Galaxy is in dynamical equilibrium: if it is allowed to be out of equilibrium, *any* distribution of stars in phase space is consistent with *any* gravitational potential – we constrain Φ by assuming that the potential is deep enough to prevent stars flying apart

in the next dynamical time but not so deep as to cause them to slump into the centre in the same period.

- Equilibrium dynamical models have much less freedom than kinematic or non-equilibrium models because their velocity structure is firmly tied to the density structure by the assumed potential. Consequently a small number of parameters suffices to specify a realistic dynamical model, and optimising the model by adjusting these parameters is reasonably straightforward.

- Observed velocity distributions are far from Gaussian but are well reproduced by quasi-isothermal DFSs.

- A properly constructed equilibrium dynamical model can be used as the foundation for the construction of non-equilibrium models via perturbation theory. In this way the model can be extended to include non-equilibrium phenomena such as spiral structure and the warp.

3. Integrals of motion

We have known since the numerical experiments of the 1960s that most orbits in Galaxy-like flattened, axisymmetric potentials admit three integrals of motion, and by the Strong Jeans Theorem the distribution function (DF) of an equilibrium model can be assumed to be a function $f(I_1, I_2, I_3)$ of these integrals. Since any function $J(\mathbf{I})$ of the integrals is obviously itself an integral of motion, there is considerable choice in what we use for arguments of the DF. One choice stands out above all others: the action integrals \mathbf{J} . The special properties enjoyed by the actions include: (i) they alone can be complemented by canonically conjugate variables θ_i to form a complete set of canonical coordinates $(\boldsymbol{\theta}, \mathbf{J})$ for phase space; (ii) the space in which the actions are Cartesian coordinates, action space, provides an undistorted compression of six-dimensional phase space in the sense that the volume of phase space occupied by orbits with actions in $d^3\mathbf{J}$ is $(2\pi)^3 d^3\mathbf{J}$; (iii) actions are adiabatic invariants so when the Galaxy's potential is slowly deepened, for example by the accretion of gas to form the disc, the orbits of stars change but their actions do not. The property of adiabatic invariance enables us to compute the effects of accretion without knowing precisely how the accretion occurred – we need to know only the initial and final potentials, not the intermediate potentials. The ability to embed the actions in a complete system of canonical coordinates is the key handling non-equilibrium aspects of the Galaxy through perturbation theory – angle-action coordinates were invented in the 19th century in order to compute the dynamics of the solar system using perturbation theory. Particle physics, condensed-matter physics, plasma physics, and celestial mechanics are all built around perturbation theory, which is not merely the means by which we compute the implications of models but provides the concepts – Feynman diagrams, phonons, spin-waves, mean-motion resonances, etc., – with which we understand the phenomena. Galactic dynamics will remain a primitive branch of physics until it too makes extensive use of perturbation theory, and our first step towards that goal must be expressing equilibrium models in terms of angle-action coordinates.

The angular momentum around the Galaxy's approximate symmetry axis L_z is one of the three actions. The best expressions we have (Binney 2010, 2012a; Sanders 2012) for the integral of motion that controls the extent of a star's excursions perpendicular to the Galactic plane are for the vertical action J_z . Consequently the only real temptation to employ an integral that is not an action is the temptation to use the energy E as the third integral rather than the radial action J_r , which controls the extent of a star's radial oscillation. For some the arguments advanced above for choosing J_r over E do

not suffice to wean them off E , and to these people we say that if your DF has the form $f(E, L_z)$ it is quite tricky to find the self-consistent gravitational potential (Prendergast & Tomer 1970; Rowley 1988). Indeed, the search for Φ proceeds iteratively – one guesses Φ , evaluates the density $\rho = \int d^3\mathbf{v} f$ then implied, solves Poisson’s equation for the corresponding potential Φ' and repeats the process until convergence. At each iteration the central potential changes, with the result that the density depends upon a different range of values of E , and the iterations converge only if some subtle scalings are employed (e.g., Binney & Tremaine 2008, §4.4.2(b)). Since actions always range from 0 for a star that rests at the bottom of the potential well to ∞ for marginally bound stars, when we adopt $f(\mathbf{J})$ the iterations converge automatically.

In the following we take the DF to have the form $f(\mathbf{J})$ and not waste time on more traditional formulations.

4. Choice of the DF

4.1. Basic DFs

Binney (2010, 2012b, hereafter B12) showed that superpositions of quasi-isothermal DFs give good fits to the Geneva-Copenhagen Catalogue and successfully predict data from the SDSS and RAVE surveys. A quasi-isothermal DF has the form

$$f_{\text{iso}}(\mathbf{J}) \propto \exp(-R_c/R_d) \exp(-\kappa J_r/\sigma_r^2) \exp(-\nu J_z/\sigma_z^2), \quad (4.1)$$

where R_d is essentially the radial scale length of the disc, $R_c(L_z)$ is the radius of a circular orbit of angular momentum L_z , $\kappa(L_z)$ and $\nu(L_z)$ are the radial and vertical epicycle frequencies of this orbit, and $\sigma_r(L_z)$ and $\sigma_z(L_z)$ are approximately equal to the radial and vertical velocity dispersions of the disc at R_c . The name “quasi-isothermal” for this DF derives from the observation that in the epicycle approximation $\kappa J_r = E_r$ is the in-plane epicycle energy and $\nu J_z = E_z$ is the energy of vertical oscillations, so the DF becomes an exponential function of these energies like the Gibbs distribution of standard statistical mechanics.

The Hipparcos data showed that the velocity dispersions of thin-disc stars grow with age τ roughly as $\tau^{0.33}$ (e.g. Aumer & Binney 2009), so Binney (2010) set

$$\sigma_i(L_z, \tau) = \sigma_i(L_z) \left(\frac{\tau + \tau_1}{\tau_T + \tau_1} \right)^{0.33}, \quad (4.2)$$

where τ_1 is a parameter that controls the velocity dispersion of the stars at birth, τ_T is the age of the oldest thin-disc stars and σ_i is essentially the present velocity dispersion at R_c . This dispersion is expected to decrease outwards through the disc, and an appropriate functional form is

$$\sigma_i(L_z) = \sigma_{i0} \exp(-R_c/R_\sigma), \quad (4.3)$$

where σ_{i0} is a number, R_σ is the radius over which the velocity dispersion falls by a factor $\sim e$. Aumer & Binney (2009) showed that the Hipparcos data are consistent with the hypothesis that the star formation rate (SFR) near the Sun has varied with time as $\exp(-t/\tau_f)$ so a reasonable form for the DF of the thin disc is

$$f_{\text{thin}}(\mathbf{J}) \propto \int d\tau \exp(\tau/\tau_f) f_{\text{iso}}(\mathbf{J}, \tau). \quad (4.4)$$

That is, the thin disc is modelled as a superposition of quasi-isothermal discs, one for each coeval cohort of stars, with the velocity dispersion of each cohort increasing with age.

B12 took the thick disc to be a single quasi-isothermal comprising exclusively old stars. The DF of the complete disc is then

$$f(\mathbf{J}) = (1 - F)f_{\text{thin}}(\mathbf{J}) + Ff_{\text{thick}}(\mathbf{J}), \quad (4.5)$$

where the individual DFs are normalised such that $\int d^3\mathbf{J} f = 1$ and F is the fraction of the mass of the disc contributed by the thick disc.

4.2. Extended DFs

In principle every observationally distinguishable class of star can have its own DF. Kinematics and chemistry are highly correlated, so stars with different metallicities must have different DFs. We can model this situation by extending the DF above to an extended distribution function (EDF), which is a function of chemical composition in addition to actions.

We start by supposing that the chemical composition of the interstellar medium (ISM) is at any given time a function of Galactocentric radius R only, and that the chemical composition of a star is the same as that of the ISM at the coordinates (R, τ) of its birth. The upper panel of Fig. 1 shows the time dependence of metallicity at several radii in the model of Schönrich & Binney (2009, hereafter SB09). We model this dependence with

$$[\text{Fe}/\text{H}](R, \tau) = F(R, \tau) \equiv F(R) + [F(R) - F_m] \left[\tanh\left(\frac{\tau_m - \tau}{\tau_f}\right) - 1 \right], \quad (4.6)$$

where from SB09 we adopt the current metallicity-radius relation

$$F(R) = \tanh\left\{0.6 - 0.082\frac{R}{\text{kpc}}\right\}, \quad (4.7)$$

which yields a linear decline of $[\text{Fe}/\text{H}]$ near the sun flattening to -1 at large R . Here τ_m is the maximum age of any star in the Galaxy, F_m is that star's value of $[\text{Fe}/\text{H}]$, and τ_f is a parameter that controls the rate of enrichment at early times. Following SB09 we adopt $\tau_m = 12$ Gyr and $F_m = -1$. The lower panel of Fig. 1 shows a reasonable fit to the SB09 model is afforded by $\tau_f = 1.98$ Gyr.

With the assumption that a star's metallicity is given by equation (4.6) with R interpreted as $R_c(L_z)$ the EDF becomes

$$f(\mathbf{J}, [\text{Fe}/\text{H}]) = \int d\tau \exp(\tau/\tau_f) f_{\text{iso}}(\mathbf{J}, \tau) \delta([\text{Fe}/\text{H}] - F(R_c, \tau)). \quad (4.8)$$

On account of churning (Sellwood & Binney 2002), the present angular momentum L_z of a star differs from its birth angular momentum L'_z by a random offset, which we assume is drawn from a Gaussian distribution with dispersion σ_L that grows with time, so

$$\sigma_L(\tau) = \sigma_{L0} \left(\frac{\tau}{\tau_m}\right)^{\gamma\tau}. \quad (4.9)$$

With churning taken into account, the EDF becomes

$$f(\mathbf{J}, [\text{Fe}/\text{H}]) = \int dL'_z \int d\tau \exp(\tau/\tau_f) \frac{e^{-(L_z - L'_z)^2/2\sigma_L^2}}{\sqrt{2\pi\sigma_L^2}} f_{\text{iso}}(\mathbf{J}', \tau) \delta([\text{Fe}/\text{H}] - F(R'_c, \tau)), \quad (4.10)$$

where $\mathbf{J}' \equiv (J_r, L'_z, J_z)$ and $R'_c \equiv R_c(L'_z)$. When we use the δ -function to execute the integral over L'_z we obtain

$$f(\mathbf{J}, [\text{Fe}/\text{H}]) = \int d\tau \exp(\tau/\tau_f) \frac{e^{-(L_z - L'_z)^2/2\sigma_L^2}}{\sqrt{2\pi\sigma_L^2}} \frac{f_{\text{iso}}(\mathbf{J}', \tau)}{|\partial F/\partial R_c| |\partial R_c/\partial L_z|}, \quad (4.11)$$

where L'_z is given by $F(R_c(L'_z), \tau) = [\text{Fe}/\text{H}]$.

5. Fitting an incomplete catalogue

To test a model by comparing it with a catalogue, we have to “observe” the model in the same way that the survey observes the Galaxy. Most of the major surveys now underway make strenuous efforts to be photometrically complete in some well-defined way. Nevertheless this completeness is achieved, if at all, only in the final data release because a host of complex constraints and considerations affect the order in which targets are selected – bright stars are likely to be selected ahead of faint ones, and in crowded fields it may be impossible to sweep up adjacent targets in the first visit to the field. Fortunately, these considerations are almost always velocity-blind in the sense that the probability that a given star is included in a particular data release is rigorously independent of its velocity. In these circumstances it is easy to test a model with a catalogue for which we have estimates of distance and chemical composition as follows.

We bin the stars spatially and chemically in any convenient way. For each star in a bin

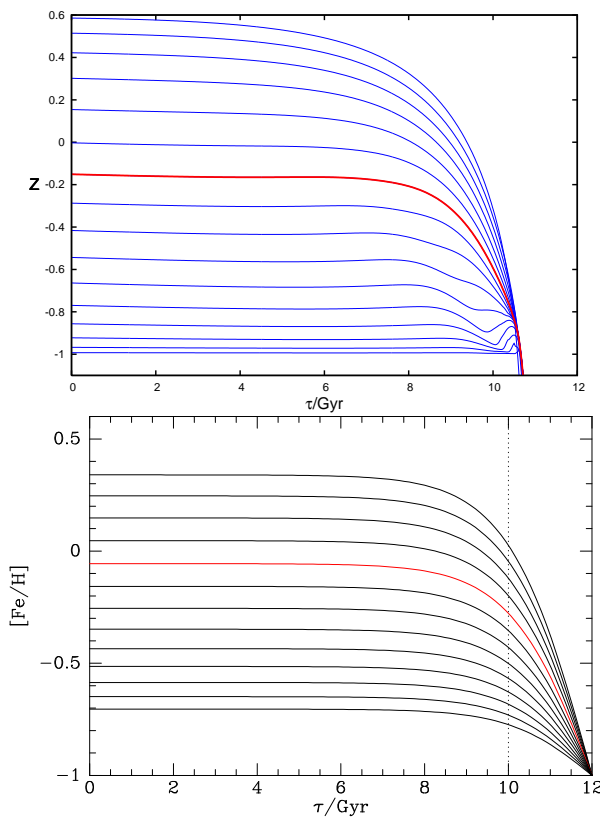


Figure 1. The upper panel shows the evolution of $[\text{Fe}/\text{H}]$ in the ISM according to the model of Schönrich & Binney (2009). Each curve corresponds to a radius that increases from top to bottom in steps of 1.25 kpc, the curve for $R = 8$ being shown in red. The lower panel shows the analytic approximation to this evolution afforded by eqs. (4.6) and (4.7). The increment in R between curves is again 1.25 kpc with the curve for $R = 8$ kpc shown in red. The region to the right of the dotted vertical line is taken to constitute the thick disc, which has the DF of a single quasi-isothermal.

we choose a hypothetical true distance s' using either a simple Gaussian distribution in s' or, more rigorously, using the a posteriori probability distribution of s' for each star that is returned by a Bayesian distance-determination algorithm (Burnett & Binney 2010; Binney et al. 2013). The probability distributions from a Bayesian algorithm are clearly to be preferred because they take into account the higher density of stars near us than further away and also distance ambiguities associated with uncertainty as to whether a star is a dwarf or some type of giant. In the same spirit we select a hypothetical true metallicity $[\text{Fe}/\text{H}]'$ by sampling the product of the model's metallicity distribution along that line of sight and the probability distribution of measurement errors in $[\text{Fe}/\text{H}]$. Once hypothetical true values of all relevant observables have been selected in this way, we sample the model's velocity distribution at the hypothesised location

$$P(\mathbf{v}) = f(\mathbf{J}(\mathbf{x}', \mathbf{v}), [\text{Fe}/\text{H}]', \dots). \quad (5.1)$$

We convert \mathbf{v} into the line of sight velocity v_{\parallel} and proper motion $\boldsymbol{\mu}$ using the hypothesised distance s' . Next we add to v_{\parallel} and $\boldsymbol{\mu}$ appropriate measurement errors before converting them back to a space velocity \mathbf{v} using the measured distance s . These velocities constitute the model's predictions for the distribution of velocities of catalogued stars in the given spatial bin. These predictions take fully into account all measurement errors, no matter how gross, in distances, velocities and metal abundances. If the measurement errors have been correctly assessed, any statistically significant discrepancy between this theoretical velocity distribution and the observed one must reflect a shortcoming of the model.

6. Metallicity-blind predictions from the GCS catalogue

B12 fitted a DF $f(\mathbf{J})$ to the Geneva-Copenhagen Catalogue (GCS) of F and G stars (Nordstrom et al. 2004; Holmberg et al. 2007) as follows. First the thin-disc DF was fitted to the histograms of U , V and W velocity components. Then the data set was augmented by the Gilmore & Reid (1983, hereafter GR83) estimates of the stellar density $\rho(z)$ at distance z from the plane, and the entire DF was fitted. Since the fits to all the data, especially the distribution of W components and the GR83 density points, were excellent, it was evident that the gravitational potential adopted is not far from the truth. However, more rigorous tests of the (DF, Φ) combination of this model are provided by using it to predict the velocity distributions of RAVE stars, which, unlike the GCS stars, extend far beyond a sphere around the Sun of radius ~ 150 pc.

Figs. 2 and 3 show results for giants. We divide the stars into those inside/outside the solar radius, and into three bins in $|z|$. The black points show histograms for $\sim 140\,000$ RAVE giants; each point's vertical bar shows the statistical error in that bin. The red points show the corresponding theoretical predictions.

Fig. 2 shows histograms for the vertical velocity component V_3 (the direction of this component changes from point to point in the (R, z) plane to track a principal axis of the velocity ellipsoid). The mean $(R, |z|)$ coordinates of the contributing stars appear in brackets in the lower centre of each panel above the error-corrected velocity dispersion in the bin (sD) and the mean velocity (mV). In all panels the red and black histograms agree nearly perfectly, even though the stars that contribute to the lower four panels lie far outside the region occupied by the GCS stars, to which the DF was fitted.

Fig. 3 shows histograms for v_{ϕ} . Although not perfect, the agreement between the red and black histograms is again impressive given that the red points are predictions rather than fits to these data. The fit becomes near-perfect if one assumes that the distances to the most remote stars have been overestimated by $\sim 20\%$.

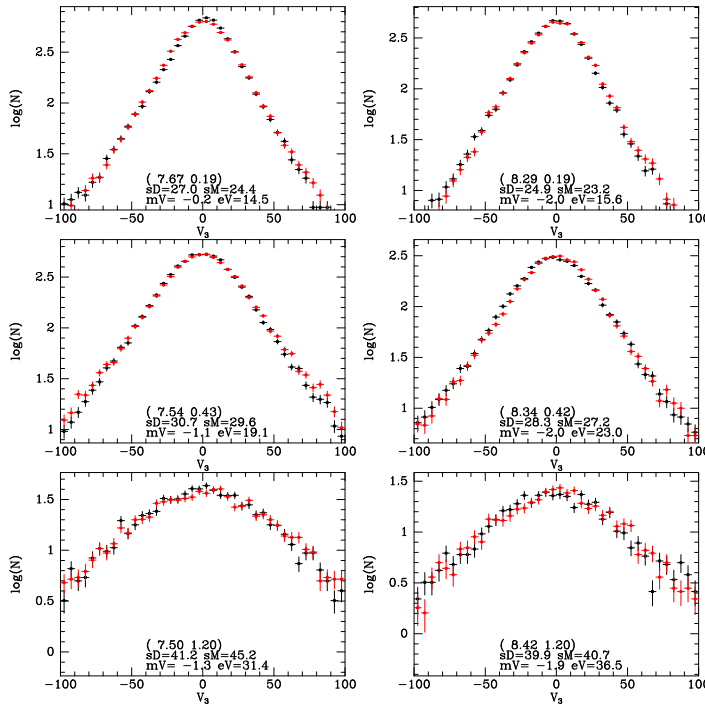


Figure 2. Vertical velocity components of giant stars in RAVE. Left column: stars with $R < R_0$, right column $R > R_0$. The red points are the prediction of the model for thin-disc stars, the black points show velocities measured by RAVE. The numbers in brackets at the bottom give the mean values of R and $|z|$ for stars in that bin.

7. Including metallicity information

In the last section we merely tested against RAVE data a previously selected basic DF. Now we report fitting an EDF to a combination of SEGUE and GCS data. In this work we include a halo described by a classical isothermal DF $f \propto \exp(-E/\sigma^2)$. The parameters of the halo, including the local density of its stars, are fixed. Its metallicity distribution is a Gaussian centred on $[\text{Fe}/\text{H}] = -1.5$ with dispersion 0.5. It contributes $\sim 0.1\%$ of local stars.

The thick disc was taken to be a single quasi-isothermal distribution with the metallicity-angular momentum relation that one gets by integrating with respect to τ within the lower panel of Fig. 1 from $\tau = 10$ Gyr to 12 Gyr. Likelihood maximisation was first used to fit the EDF of the thick disc to G dwarfs in the DR9 SEGUE catalogue with $R > R_0$ and z in (1.5, 2) kpc. $N \simeq 50$ possible values of \mathbf{x} , \mathbf{v} and $[\text{Fe}/\text{H}]$ were chosen for each star α from that star's error distribution. For each such coordinate set the ratio

$$n(\mathbf{v}_j) \equiv \frac{f_{\text{thick}}(\mathbf{x}_j, \mathbf{v}_j, [\text{Fe}/\text{H}]_j)}{\int d^3\mathbf{v} f_{\text{thick}}(\mathbf{x}_j, \mathbf{v}, [\text{Fe}/\text{H}]_j)} \quad (7.1)$$

is the normalised probability density of the assigned velocity given the position and metallicity assignments. Crucially, by dividing by the velocity integral we have made $n(\mathbf{v}_j)$ insensitive to the spatial and metallicity coordinates, and therefore to the survey's

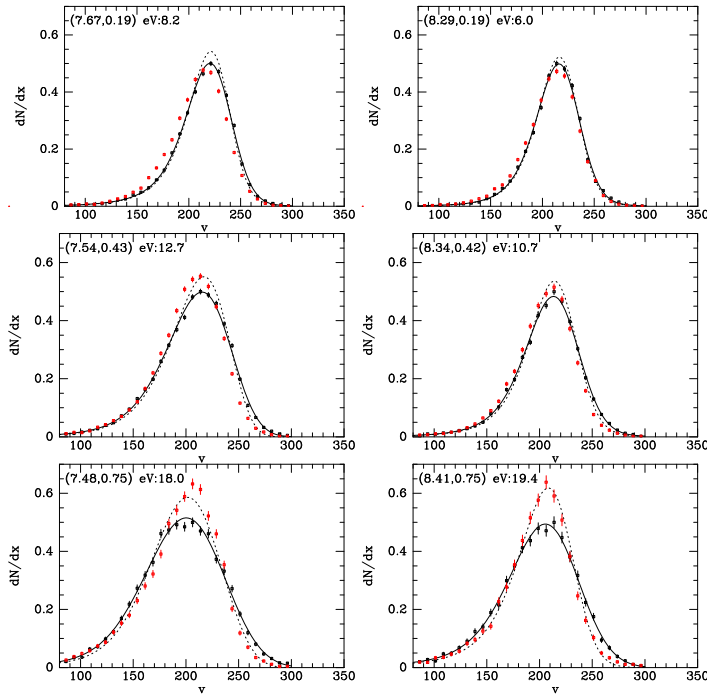


Figure 3. v_ϕ components of RAVE giants. Left column: stars with $R < R_0$, right column $R > R_0$. The red points are the prediction of the model, the black points show velocities measured by RAVE. The numbers in brackets at top left give the mean values of R and $|z|$ for stars in that bin followed by the mean observational error. The dotted curves show models of the underlying error-corrected distribution and the black curves show the result of convolving these distributions with the stated errors.

selection function. The average

$$p_\alpha \equiv \frac{1}{N} \sum_{j=1}^N n(\mathbf{v}_j) \quad (7.2)$$

over all randomly sampled velocities \mathbf{v}_j is a statistically more stable measure of the probability of the star's measured velocity (around which the \mathbf{v}_j cluster) that inherits the same insensitivity to the selection function. In order to ensure that the density profile $\rho(z)$ of the thick disc is appropriate, the parameters of the thick-disc EDF were chosen by maximising the function

$$\mathcal{L} = \sum_{\text{stars } \alpha} p_\alpha - \sum_{z > 1.3 \text{ kpc}} \left| \frac{\log_{10}[\rho_{\text{GR}}(z)/\rho_{\text{DF}}(z)]}{\sigma_{\text{GR}}(z)} \right|^2, \quad (7.3)$$

where ρ_{GR} is the density profile from GR83, σ_{GR} are the errors in $\log_{10}(\rho_{\text{GR}})$, and ρ_{DF} is the density profile predicted by the EDF.

After pinning down the parameters of the thick-disc EDF in this way, the GCS velocities, with $[\text{Fe}/\text{H}]$ values from Casagrande et al. (2011) were used to maximise a log likelihood similar to equation (7.3) but (a) using all the GR83 points in the sum over z , and (b) with n in eq. (7.1) made sensitive to $[\text{Fe}/\text{H}]$ in addition to \mathbf{v} by adding integration over

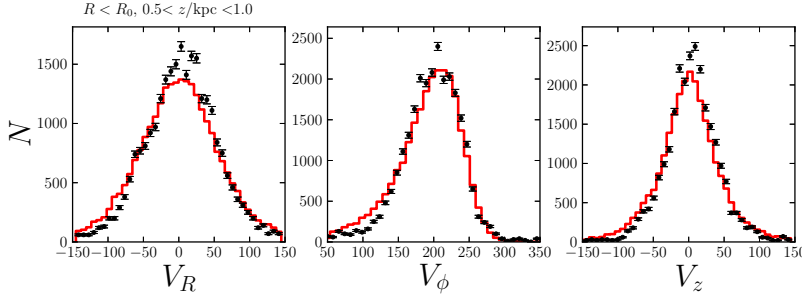


Figure 4. Red histograms: predicted velocity distributions for SEGUE G dwarfs in the spatial bin $R < R_0, 0.5 < |z| < 1$.

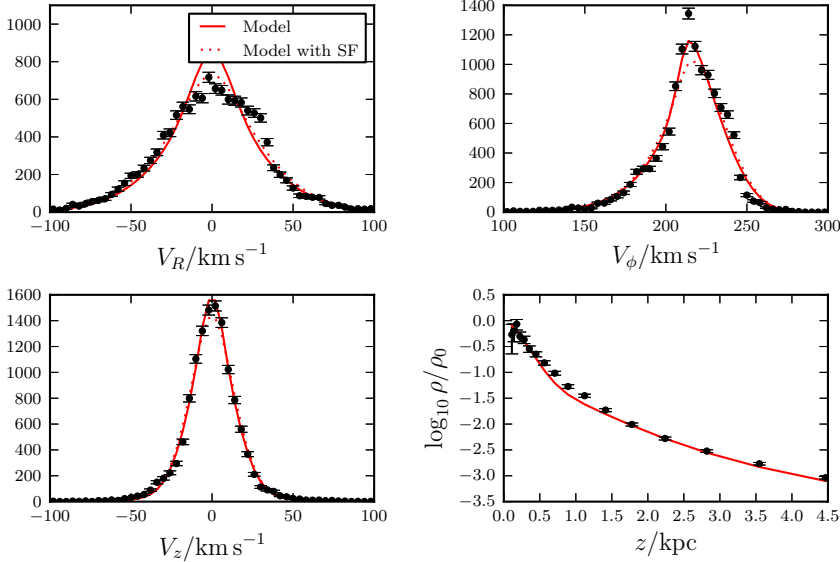


Figure 5. Fits of the model to the three velocity histograms of GCS stars and the Gilmore-Reid density profile.

[Fe/H] to the denominator

$$n(\mathbf{v}_j) \equiv \frac{f_{\text{all}}(\mathbf{x}_j, \mathbf{v}_j, [\text{Fe}/\text{H}]_j)}{\int d^3\mathbf{v} \int [\text{Fe}/\text{H}] f_{\text{all}}(\mathbf{x}_j, \mathbf{v}, [\text{Fe}/\text{H}])}, \quad (7.4)$$

where f_{all} is the complete EDF rather than just of just that of the thick disc.

Fig. 4 shows that the final model provides reasonable if not spectacular fits to the velocities of SEGUE dwarfs that were not used in the fitting procedure. The lower-left panel of Fig. 5 shows that the model provides an excellent fit to the distribution of W components of GCS stars, while the upper two panels show that the fits to the U and V components are imperfect at low velocities, presumably on account of the prominence of streams near the origin of the (U, V) plane (Dehnen 1998).

Our fitting procedure yields the joint probability distributions of the parameters of each disc. We do not have space to describe these distributions fully here, but we note a few points:

- The thick disc is hotter vertically than horizontally: $43 \text{ km s}^{-1} \simeq \sigma_{r0} < \sigma_{z0} \simeq$

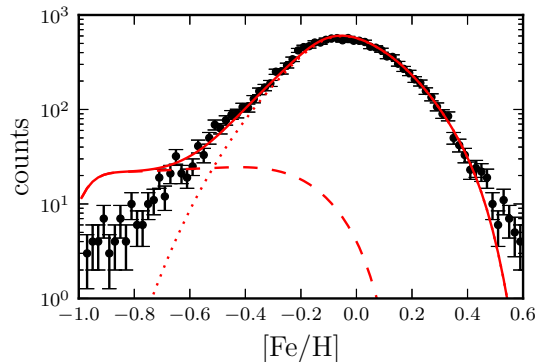


Figure 6. Data points: the metallicity distribution of the GCS from Casagrande et al. (2011). Red curve the distribution predicted by fitting the thick disc to the SEGUE G-dwarf distribution and then adding the thin disc. The red dashed curve shows the metallicity distribution of the SEGUE stars.

53 km s^{-1} . The velocity dispersion parameters of the thin disc are as expected ($37 \text{ km s}^{-1} \simeq \sigma_{r0} > \sigma_{z0} \simeq 23 \text{ km s}^{-1}$).

- The thick-disc EDF has a small scale length parameter ($R_d \lesssim 2.5 \text{ kpc}$). However, this parameter describes the distribution of birth radii of stars, and on account of strong radial migration described by the parameter σ_L in equation (4.9), the present distribution of thick-disc stars would be described by a significantly larger scale length $\sim 3.5 \text{ kpc}$.

- The scale length parameter of the thin disc is larger than that of the thick disc ($\sim 3.5 \text{ kpc}$). The spatial distribution of thin-disc stars is broadened by radial migration, even if not to the same extent as in the thick disc, so the current scale length is at the upper end of former estimates. The thin disc has a remarkably large value, $R_\sigma \gtrsim 15 \text{ kpc}$, of the scale length on which the dispersions decrease radially.

- The thick disc contributes $\sim 9\%$ of local stars, a value that is smaller than those ($\sim 13\%$ and 20%) estimated by Juric et al. (2008) and Fuhrmann (2011) but a factor of 3 larger than the original estimate of GR83. Given that the model density profile $\rho(z)$ falls below the GR83 points in the range $0.5 < |z|/\text{kpc} < 1.5$ (lower right-hand panel of Fig. 5), the normalisation of the thick disc may be too low. However, Fig. 6 shows that the metallicity distribution of the GCS stars provide a contrary indication: when the thick-disc normalisation is large enough to fit the GR83 points, the GCS metallicity distribution shows fewer metal-poor stars than the SEGUE data require. Juric et al. (2008) derived a profile $\rho(z)$ from the SDSS data that is slightly less steep than the GR83 data, so using this profile would raise the normalisation of the thick disc's contribution to the EDF and thus exacerbate the conflict with the GCS metallicity distribution.

How serious is our inability to fit the metal-weak tail of the GCS metallicity distribution simultaneously with the GR83 density profile and the SEGUE metallicity distribution? Possible explanations include: (i) One or both of the GCS and SEGUE metallicity scales is wrong; (ii) During the formation of the thick disc, the star-formation rate varied rapidly, with the consequence that the actual metallicity distribution in the thick disc is not adequately approximated by the one we have gleaned from the right-hand end of the lower panel of Fig. 1 under the assumption that of a constant SFR. (iii) The thick disc's DF is not approximately quasi-isothermal. Specifically, if the DF were not a monotonically decreasing function of J_z , it would be possible to have the required number of metal-poor stars at $|z| \sim 1.75 \text{ kpc}$ without exceeding the number seen at $z \sim 0$ because the density profile $\rho(z)$ of the thick disc could be non-decreasing at $|z| \lesssim 1 \text{ kpc}$. Two strong objections

can be raised to this fix: (a) the proposed density profile conflicts with the conclusion of Bovy et al. (2012) that mono-abundance populations have double-exponential density profiles, as predicted by quasi-isothermal DFS; (b) if, as seems likely, the thick disc formed by stars being scattered from near-circular orbits during an early disorderly phase in the life of the Galaxy, the DF must decrease in the direction that stars diffused, namely that of increasing J_z . For these reasons we consider it unlikely that the conflict arises from the assumed form of the EDF and is more likely to arise from either differences in metallicity scales or rapid early fluctuation in the SFR.

8. Conclusions

Equilibrium dynamical models are crucial for the scientific exploitation of surveys. We have given two examples of their use. First we have shown that a DF fitted to the velocity distribution of local stars plus the GR83 density profile predicts the velocity distributions of RAVE stars with remarkable success given that most RAVE stars lie far from the Sun. Second we have introduced an analytic EDF to model the correlations between kinematics and chemistry. The EDF is inspired by a particular picture of disc formation but its validity is ultimately independent of its original physical motivation. We fitted this EDF to a combination of the SEGUE data for G dwarfs seen ~ 1.75 kpc from the plane and the local GCS stars. The resulting EDF makes reasonably successful predictions for kinematic data not used in the fitting process, but provides an unsatisfactory fit to the distribution in $[\text{Fe}/\text{H}]$ of the GCS stars in the sense of requiring more low-metallicity stars than observed. We discussed possible resolutions of this discrepancy, and none is very attractive.

The fitting process suggests that for the thick disc the ratio of velocity dispersions σ_r/σ_z is less than unity, whereas for the thin disc it much exceeds unity.

References

- Aumer, M. & Binney, J., 2009, MNRAS, 397, 1286
 Binney, J., 2010, MNRAS, 401, 2318
 Binney, J., 2012a, MNRAS, 426, 1328
 Binney, J., 2012b, MNRAS, 426, 1342 (B12)
 Binney et al., 2013, MNRAS, to be submitted
 Binney, J., & Tremaine, S., 2008, *Galactic Dynamics*, Princeton University Press, Princeton
 Bovy J., Rix H.-W., Liu C., Hogg D.W., Beers T.C., Lee Y.S., 2012, ApJ, 753, 148
 Burnett, B. & Binney J., 2010, MNRAS, 407, 339
 Casagrande, L., Sch'önrich, R., Asplund, M., Cassisi, S., Ramirez, I., Meléndez, J., Bensby, T., & Feltzing, S., 2011, A&A, 530, 138
 Dehnen W., 1998, AJ, 115, 2384
 Fuhrmann K., 2011, MNRAS, 414, 2893
 Gilmore G., Reid N., 1983, MNRAS, 202, 1025
 Holmberg J., Nordström B., Andersen J., 2007, A&A 475, 519
 Juric et al., 2008, ApJ, 673, 864
 Nordstrom, B., Mayor M., Andersen J., Holmberg J., Pont F., Jorgensen B.R., Olsen E.H., Udry S., Mowlavi N., 2004, A&A, 418, 989
 Prendergast, K.H., & Tomer, E., 1970, AJ, 75, 674
 Robin A., Reylé C., Derrière S., Picaud S., 2003, A&A, 409, 523
 Rowley, G., 1988, ApJ, 331, 124
 Sanders, J.L., 2012, MNRAS, 426, 128
 Sch'önrich, R. & Binney, J., 2009, MNRAS, 396, 203 (SB09)
 Selwood, J.A. & Binney, J., 2002, MNRAS, 336, 785

Discussion

REDDY: Your model shows clear separation of the thin and thick discs at 10 Gyr. I think the thick disc evolves beyond the “knee” and hence there must be many metal-rich young thick-disc stars younger than 10 Gyr

BINNEY: Although our model involves age as a parameter that controls dispersion and chemistry, we don’t have – and have no prospect of getting – the observational ability to distinguish stars with ages say one Gyr either side of our brutal division of the disc into thin and thick at τ_T . So in practice it would make no difference if there were overlap between the ages of stars in the two discs.

RIX: Why do you consider the present-day velocity dispersions of disc (sub-) populations mostly (or exclusively) as a result of heating. Could they in good part not be a “birth property”?

BINNEY: We know that much or all of the thin disc has acquired random velocity through stochastic acceleration by fluctuations in the gravitational field. So I submit that the correct procedure scientifically is to assume that *all* disc stars were born on near circular orbits. This assumption may be false, but I want the data to demonstrate that, which they can do only if I make the assumption and show it leads to conflict with the data.

MINCHEV: 1. You showed that the ratio of vertical to radial velocity dispersions is larger for the thick disc stars. Could this be seen as an indication that the Milky Way disc was affected by mergers at high redshift? 2. Is it possible to predict the past evolutionary history of the MW disc using the DF approach?

BINNEY: 1. Before we speculation as to how the Galaxy got to its present configuration, we should establish beyond reasonable doubt how it is *presently* configured and how it works. I find it distracting to be drawn into speculation about origins at this early stage. 2. The DF of an equilibrium model, by definition, has the same dynamical past as future. Information about the past, if it lingers, is encoded in the distribution of stars in angle space, which I’m deliberately assuming to be uniform. In reality it will be non-uniform. The key point is that you cannot hope to make progress with probing the past until you have achieved clarity about the present.

CHEN YUN-TENG: How to interpret discrepancy between observables and models? How to choose to quantify the comparison of models and observations.

BINNEY: Since we are currently comparing theoretical and measured 1-d histograms, we could use either χ^2 or the Kolmogorov-Smirnov measures of discrepancy. Actually Jason Sanders is using χ^2 and I have used “ χ^2 by eye”. Really we should be comparing densities in full 3d velocity space, and for that I suppose only χ^2 is feasible.

RITTER: The comparison to external data sets has shown that there is pretty much no connection between RAVE α enhancements and α enhancements derived from high-resolution, high SNR spectra. This could explain some of the discrepancies between the RAVE data and the model. I suggest you use the α enhancements from Boeche’s element abundance catalogue instead, which should be more reliable than the official RAVE values.

BINNEY: We *are* using the Boeche et al. values. All the results were restricted to [Fe/H].